




# Unrecognized role of claudin-10b in basolateral membrane infoldings of the thick ascending limb

Catarina Quintanova<sup>1</sup>  | Nina Himmerkus<sup>1</sup> | Samuel L. Svendsen<sup>2</sup> | Otto von Schwerdtner<sup>1</sup> | Cosima Merkel<sup>1</sup> | Lennart Pinckert<sup>1</sup> | Kerim Mutig<sup>3,4</sup> | Tilman Breiderhoff<sup>5</sup> | Dominik Müller<sup>5</sup> | Dorothee Günzel<sup>6</sup>  | Markus Bleich<sup>1</sup> 

<sup>1</sup>Institute of Physiology, Christian-Albrechts-University, Kiel, Germany

<sup>2</sup>Department of Biomedicine, Physiology, Aarhus University, Aarhus, Denmark

<sup>3</sup>Department of Translational Physiology, Charité-Universitätsmedizin, Berlin, Germany

<sup>4</sup>Department of Pharmacology, I.M. Sechenov First Moscow State Medical University (Sechenov University), Moscow, Russian Federation

<sup>5</sup>Department of Pediatrics, Division of Gastroenterology, Nephrology, and Metabolic Medicine, Charité-Universitätsmedizin, Berlin, Germany

<sup>6</sup>Clinical Physiology/Nutritional Medicine, Charité-Universitätsmedizin, Berlin, Germany

## Correspondence

Catarina Quintanova, Physiologisches Institut, Herman-Rodewald-Straße 5, 24118 Kiel, Germany.

Email: [c.quintanova@physiologie.uni-kiel.de](mailto:c.quintanova@physiologie.uni-kiel.de)

Catarina Quintanova and Nina Himmerkus contributed equally.

[Correction added on September 17, 2022, after first online publication: Affiliation 4 was added for Kerim Mutig.]

## Abstract

Claudin-10b is an important component of the tight junction in the thick ascending limb (TAL) of Henle's loop and allows paracellular sodium transport. In immunofluorescence stainings, claudin-10b-positive cells exhibited extensive extra staining of basolateral, column-like structures. The precise localization and function have so far remained elusive. In isolated cortical TAL segments from C57BL/6J mice, kidney-specific claudin-10 knockout mice (cKO), and respective litter mates (WT), we investigated the localization and protein expression and function by fluorescence microscopy and electrophysiological measurements. Ultrastructural analysis of TAL in kidney sections was performed by electron microscopy. Claudin-10b colocalized with the basolateral Na<sup>+</sup>-K<sup>+</sup> ATPase and the Cl<sup>-</sup> channel subunit barttin, but the lack of claudin-10b did not influence the localization or abundance of these proteins. However, the accessibility of the basolateral infolded extracellular space to ouabain or fluorescein was increased by basolateral Ca<sup>2+</sup> removal and in the absence of claudin-10b. Ultrastructural analysis by electron microscopy revealed a widening of basolateral membrane infoldings in cKO in comparison to WT. We hypothesize that claudin-10b shapes neighboring membrane invaginations by *trans* interaction to stabilize and facilitate high-flux salt transport in a water-tight epithelium.

## KEYWORDS

claudin-10, epithelium, ion transport, TAL

## INTRODUCTION

The thick ascending limb (TAL) of Henle's loop has a critical role in salt transport and urine concentration. It is responsible for the reabsorption of approximately 30% of the filtered sodium chloride and is essential to calcium and magnesium homeostasis.<sup>1</sup> The basic transcellular transport mechanisms in the TAL involve the cotransport of Na<sup>+</sup>, K<sup>+</sup>, and 2 Cl<sup>-</sup> across the luminal membrane by NKCC2. The luminal renal outer medullary K<sup>+</sup> channel is required for the recycling of K<sup>+</sup>

and sustains the activity of NKCC2.<sup>2,3</sup> Na<sup>+</sup> is pumped out of the cell through the basolateral Na<sup>+</sup>-K<sup>+</sup> ATPase (NKA).<sup>4,5</sup> In parallel, Cl<sup>-</sup> exits by the basolateral Cl<sup>-</sup> channel ClC-K<sub>a/b</sub> with its subunit barttin.<sup>6</sup> The separation of luminal and basolateral ion transport properties generates a lumen-positive potential that drives the paracellular transport of Na<sup>+</sup>, Ca<sup>2+</sup>, and Mg<sup>2+</sup> (Ref. 2).

The paracellular pathway is built by tight junctions (TJs). The major components of the TJ strands are claudins and the different composition in claudins determines TJ permeability or barrier function.

This is an open access article under the terms of the [Creative Commons Attribution-NonCommercial-NoDerivs](https://creativecommons.org/licenses/by-nc-nd/4.0/) License, which permits use and distribution in any medium, provided the original work is properly cited, the use is non-commercial and no modifications or adaptations are made.

© 2022 The Authors. *Annals of the New York Academy of Sciences* published by Wiley Periodicals LLC on behalf of New York Academy of Sciences.

Claudins are tetraspan transmembrane proteins with two extracellular loops and intracellular N- and C-termini.<sup>7</sup> Claudins interact through their extracellular loops and form cis-interaction with claudins in the membrane of the same cell or *trans* interactions with claudins of the neighboring cell.<sup>7</sup> Claudins can form charge- and ion-selective pores in the lateral space.<sup>7,8</sup> The major claudins expressed in the TAL are claudin-3, -10, -14, -16, and -19.<sup>7-9</sup> In the case of claudin-10, only isoform b is localized in the TJs of the TAL and forms a water-impermeable cation-selective channel.<sup>10</sup> Claudin-10b is lost in the TAL of kidney-specific cadherin-16 Cre (Ksp-Cre) claudin-10 knockout mice.<sup>11</sup> As a phenotypic consequence, mice display hypermagnesemia and nephrocalcinosis which can be explained by the impaired Na<sup>+</sup> permeability, which is replaced by an increased Ca<sup>2+</sup> and Mg<sup>2+</sup> permeability and reabsorption. In addition, these mice showed modest polyuria.<sup>11,12</sup> Also in humans, “claudinopathies” caused by claudin-10 mutations have been described, with nearly all patients displaying renal dysfunction with hypermagnesemia, hypokalemia, and hypocalciuria, besides external manifestations due to claudin-10 being localized in other epithelia (salivary, sweat, and lacrimal glands).<sup>13,14</sup> Interestingly, claudin-10b does not interact with other members of the claudin family in the TAL. This is reflected by a mosaic pattern in the cortical TAL segment (cTAL) TJ, where TJs either exclusively express claudin-10b or the other claudins, with the tricellular junction as the switching point.<sup>15</sup>

Another peculiar feature of claudin-10b is its ability to localize in membranes outside the TJ. This has been observed after overexpression in cell cultures.<sup>16</sup> Also, claudin-10b is localized basolaterally in the native TAL.<sup>11</sup> Electron microscopy of TAL cells shows that the basolateral membrane possesses invaginations reaching deep into the cell body, almost up to the lumen membrane.<sup>17</sup> Mainly mitochondria are situated between these infoldings, and this alternating pattern of cell membranes, mitochondria, and fluidic spaces leads to basolateral stripes similar to the ones observed in proximal tubule (PT).<sup>18</sup> However, the interdigitations between neighboring cells as seen in PT, where cells are highly interlaced, are less distinctive and occur only in boundary areas.<sup>19</sup> Similar to distal convoluted tubule (DCT),<sup>4,18-21</sup> TAL infoldings increase basolateral membrane surface and allow a close colocalization of the mitochondrial energy source with the Na<sup>+</sup>-K<sup>+</sup> ATPase to fuel transcellular transport. In addition, the architecture of the infolded spaces allows the development of a specific microenvironment and fluid composition.<sup>18</sup>

Several members of the claudin family have been identified outside the TJs; however, so far, little is known about their role.<sup>22</sup> It has been hypothesized that extra-junctional claudin expression may function as a pool of proteins that can be recruited to the TJs.<sup>22-25</sup> It may also function as an additional permeability barrier. In the stomach, where paracellular H<sup>+</sup> diffusion must be hindered sufficiently, there are highly packed TJ strands followed by a broader belt of a more loosely composed TJ network.<sup>26</sup> Claudin-1, -2, -3, and -4 have been localized in the nucleus of several cancer cells, which suggests regulation of gene transcription.<sup>22</sup> Claudin-3 in bronchial epithelial cells can translocate to the nucleus after transforming growth factor beta (TGF- $\beta$ ) induction.<sup>27</sup> Recently, we could show that claudins can localize in the luminal membrane and that phosphorylated claudin-16

in the DCT acts as a regulator of a luminal cation channel, while unphosphorylated claudin-16 is found only in the TAL.<sup>28</sup>

These yet rather random findings might indicate that there is much more behind claudins than suggested by their classical localization to the TJ.<sup>22,25</sup> In this study, we investigate the role of claudin-10b in basolateral membrane infoldings of the TAL using histological and functional approaches in wild-type and Ksp-Cre claudin-10 knockout mice.

## METHODS

### Animals

Animal experiments were approved by the Institutional Animal Research and Care Committee (V312-72241.121-2). Male and female C57BL/6J as well as kidney-specific (Ksp-Cre) claudin-10 knockout animals (*Cldn10<sup>fl/fl</sup>* ksp cre+, abbreviated as cKO) and their litter mates (*Cldn10<sup>fl/fl</sup>*, here abbreviated as WT, C57BL/6N background)<sup>11</sup> were used for the experiments. Animals were fed *ad libitum* and housed under a 12-h light cycle at room temperature and standard humidity.

### Enzymatic tubule dissection

Mice were euthanized and kidneys were quickly removed and sliced to obtain enzymatic tubule suspension as described in Ref. 29. Incubation solution for tubules: 140 mM NaCl, 0.4 mM KH<sub>2</sub>PO<sub>4</sub>, 1.6 mM K<sub>2</sub>HPO<sub>4</sub>, 1 mM MgSO<sub>4</sub>, 10 mM Na-acetate, 1 mM  $\alpha$ -ketoglutarate, 1.3 mM calcium gluconate, 25 mg/L DNase I, 375 mg/L glycine, and 48 mg/L trypsin inhibitor. Collagenase II (2 mg/ml) and a thermomixer (Eppendorf, 850 rpm, 37°C) were used for dissociation. For tubular sorting, the incubation solution was supplemented with 500 mg/L albumins. Tubules (nephron segments) were isolated at 4°C, according to their morphological characteristics.<sup>29</sup> Tubules were either placed directly on microscope slides (polylysine adhesion slides, Thermo Scientific) or collected on ice and supplemented with 5 $\times$  Laemmli buffer and stored at -20°C for western blot analysis (approximately: 100 glomeruli (G), 20 proximal convoluted tubules (PCTs), 20 proximal straight tubules (PSTs), 80 cTALs, 50 DCTs, and 30–40 collecting ducts (CDs)).

### Immunofluorescence

An antigen retrieval protocol called “slow cooking” (see below) was established to allow immunofluorescence staining of basolateral infolding proteins. cTALs were fixed on microscope slides with 4% paraformaldehyde for 7 min. Afterward, tubules were washed with PBS-T (0.3% Triton X-100 in phosphate-buffered saline) and incubated with 10 mM sodium citrate (pH 6) for 3 h at 70°C. Tubules were washed with PBS-T and exposed to primary antibody (Table S1) in PBS-T + 5% BSA overnight at 4°C. Secondary antibody (Table S1) was incubated for 1–2 h after extensive washing with

PBS-T. Confocal, Airyscan, and stimulated emission depletion (STED) images were acquired using Zeiss LSM 780 and LSM 880 confocal laser-scanning microscopes (excitation laser: 488, 594, and 633 nm), both equipped with an Airyscan unit; and with Abberior STEDYCON and Expert Line microscopes (laser: 775 nm; excitation laser: 488 and 640 nm), respectively. Image J software (National Institutes of Health) was used to determine the approximate claudin-10b-positive cTAL proportion by dividing claudin-10b-positive length regions by the total outer length of middle sections of cTAL images (Figure S2A). The NKA intensity ratio [positive cells/negative cells] was calculated for individual cTAL images by measuring and dividing the mean of the integrated intensities of NKA staining of several either claudin-10b-positive or -negative regions (Figure S2A).

## Western blot analysis

Segments of the nephron were analyzed after denaturation at 95°C for 5 min by electrophoresis on 6.5% stacking, 10 or 12.5% separating SDS-polyacrylamide gels and transferred to a nitrocellulose membrane. The membranes were blocked with a 5% BSA solution in PBS-Tween (0.1%) and incubated with the primary antibody (Table S1) overnight at 4°C. The blot was then incubated with the horseradish peroxidase (HRP)-conjugated anti-rabbit IgG and anti-mouse IgG for 1 h at room temperature (Table S1). A chemiluminescent kit (GE Healthcare) was used for protein detection with the ChemiDoc MP (Bio-Rad Laboratories). Bands were analyzed using Image Lab software (Version 5.0, Bio-Rad Laboratories).

## Ouabain inhibition experiments

Manually isolated cTAL segments were dissected and microp-erfused using a double-barreled perfusion pipette as described previously.<sup>12,30,31</sup> All measurements were performed at 37°C. The length and diameter of cTAL were obtained from digitized images. The cTALs were placed in control solution (in mM): 145 mM NaCl, 0.4 mM KH<sub>2</sub>PO<sub>4</sub>, 1.6 mM K<sub>2</sub>HPO<sub>4</sub>, 1 mM MgCl<sub>2</sub>, 1.3 mM calcium gluconate, 5 mM glucose, pH 7.4, and perfused with control solution. The first barrel was used for fluid exchange and voltage measurement, and the second barrel for constant current injection (13 nA) via the silver wire electrode. The transepithelial resistance was estimated using the cable equation and the equivalent short-circuit current was calculated according to Ohm's law. For concentration-response experiments, ouabain was applied in increasing concentrations (10, 30, 100, and 300 μM) at the basolateral side, and furosemide was applied luminally (50 μM) after wash-out to fully inhibit transepithelial transport. For relative inhibition speed measurements, a canyon-shaped bath with a high flow rate was used to allow laminar flow and fast bath exchange rates. After stabilization of the lumen positive potential, a current injection was interrupted and chart recorder speed was increased (from 0.2 to 0.5 mm/s) to precisely visualize voltage changes after ouabain application. After reaching a plateau of inhibition, ouabain was removed, the chart recorder speed turned back to 0.2 mm/s, and

the current injection continued. Wash-out and viability of cTAL were checked by transepithelial voltage ( $V_{te}$ ), transepithelial resistance  $R_{te}$ , and equivalent short-circuit current  $I'_{sc}$ .<sup>30</sup> Relative inhibition rates of ouabain inhibition (wash-in) and disinhibition (wash-out) were measured from the slope of linear voltage change (mV/min). To normalize for the differences in  $V_{te}$  between cTAL, this value was then divided by the maximal inhibition in the presence of 100 μM ouabain in mV, indicated as  $V_{te}$  (inhib.).

## Fluorescein diffusion measurements

Manually dissected cTALs were transferred into the bath chamber on the stage of a Zeiss LSM 510 Meta microscope and perfused by a glass pipette perfusion system with one barrel used for fluid exchange, using a control solution (see above) on both sides. The perfused cTALs were stained by incubation with MitoTracker Deep Red FM (100 nM; Thermofisher Scientific) for 10 min in the control solution. After staining, the cTALs were washed to remove the nonretained dye. For subsequent fluorescein diffusion experiments, different basolateral solutions (control and Ca<sup>2+</sup>-free solutions) were applied and the response was recorded by a Zeiss LSM 510 Meta. For the Ca<sup>2+</sup> depletion experiment, the cTALs were superfused for 2 min with 5 mM EGTA (ethylene glycol-bis(β-aminoethyl ether)-N,N,N',N''-tetraacetic acid; Ca<sup>2+</sup> chelator) replacing calcium gluconate in the control solution. As fluorescence values were too high and the wash-in and wash-out phases too fast to be recorded, the remaining fluorescence 2 min after return to fluorescein-free solutions was determined as a measure of basolateral extracellular fluorescein trapping. In Protocol 1, the remaining fluorescein was compared between control and Ca<sup>2+</sup>-free conditions in both WT and cKO cTALs. In Protocol 2, Ca<sup>2+</sup> was readded to the basolateral solution prior to fluorescein wash-out to potentially "trap" the fluorescein in the basolateral space.

## Electron microscopy

For morphological evaluation of TALs, kidneys of WT and claudin-10-deficient mice ( $n = 3$  each) were fixed by *in vivo* perfusion under pentobarbital sodium anesthesia (LAGESO permission G0220/12). The perfusion was performed retrogradely through the abdominal aorta using PBS adjusted to 330 mOsm with sucrose (pH 7.4, for 30 s) followed by 3% paraformaldehyde in PBS (for 5 min). The kidneys were removed, cut into slices, and processed for embedding in Epon. After contrasting, ultrathin sections from outer medullary zones were evaluated by transmission electron microscopy using a Zeiss LEO 906, and TAL profiles were compared between the two genotypes by taking electron microscope TAL images.

## Statistics

Statistical analysis was performed using GraphPad Prism 7.05 and 8.4.3 software (GraphPad Software, San Diego, CA, USA,

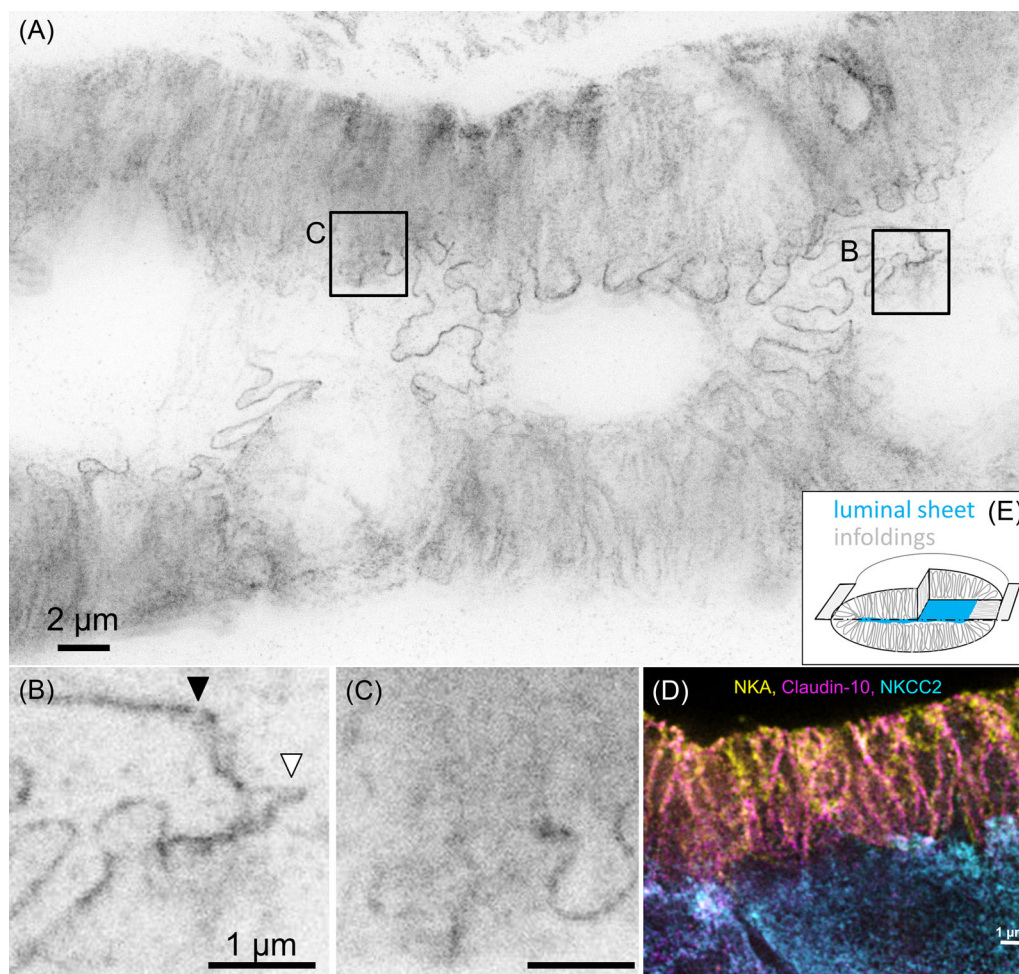


**FIGURE 1** Expression of claudin-10. (A) Overview of isolated murine cTAL tubule that was stained with claudin-10 antibody and acquired by STED microscopy. (B,C) Detailed images of claudin-10 expression in the TJ strands and intracellular compartments. (B) Claudin-10 localizes to the TJs in a broad band of several parallel strands (black arrowhead) or more individual strands (white arrowhead). (C) Expression of claudin-10 along the infoldings of the basolateral membrane (dotted line) can be traced from the basolateral membrane almost reaching the lumen. (D) Immunofluorescence of NKA (yellow), claudin-10 (magenta), and NKCC2 (cyan) was obtained by STED confocal microscopy. Claudin-10 and NKA were identified in the same structures, but not always colocalizing. Nevertheless, it was possible to recognize that the infoldings went deep into the cell, almost reaching the luminal surface where NKCC2 was localized in the luminal membrane. NKCC2, due to the collapse of the lumen, was observed as a sheet. (E) Sketch representing a collapsed tubule seen in the horizontal plane with the NKCC2 sheet (blue).

[www.graphpad.com](http://www.graphpad.com)). cTALs were used as technical replicates and a nested *t*-test was used to compare between two groups. For multiple testing (four groups, ouabain-relative inhibition speed), nested one-way ANOVA with Sidak's multiple comparisons test was performed. For western blot analysis, an unpaired *t*-test was performed between WT and cKO. Data are shown as scatter plots with all data points (all cTALs) with mean  $\pm$  SEM.

## RESULTS

### Localization of claudin-10b in cTAL

cTAL was analyzed for the expression of claudin-10b in isolated single tubules by immunofluorescence. Figure 1A shows an overview of a STED image of claudin-10b in the cTAL. In the TJ, it marks the typi-

cal meandering pattern described for highly transporting epithelia.<sup>11,15</sup> In addition, claudin-10b was also localized to extra-junctional structures. As depicted in detail in Figure 1B, claudin-10b TJs are presented in a broadband (black arrowhead). This result agrees with previous freeze-fracture studies of the TAL TJs that showed that the TJ is composed of several strands in parallel, with a total network depth of 0.1  $\mu$ m (estimated by Kottra and Frömter, 1983).<sup>32</sup> The resolution of the STED images (20 nm) was still not high enough to resolve these highly packed bands representing most likely up to 10 parallel single strands.<sup>32</sup> Occasionally, separated strands and branching were visible (white arrowhead). Outside of the TJ, claudin-10b staining revealed a dotted pattern organized in column shape (dotted line; Figure 1C) that could be followed from the basement membrane toward the luminal side, therefore, most likely situated in basolateral membrane infoldings. Both NKA and claudin-10b displayed a dotted but not completely overlapping pattern along the infolding membrane (Figure 1D).



The additionally performed NKCC2 staining in the collapsed tubule was partially in close proximity to the infoldings and was observed as a sheet as the TAL lumen was collapsed (Figure 1D,E).

### Colocalization of claudin-10b with Na<sup>+</sup>-K<sup>+</sup>-ATPase and barttin in the cTAL

To further analyze the extra-junctional localization of claudin-10b, triple immunofluorescence was performed with known proteins of the basolateral membrane. We confirmed claudin-10b localization in the TJs and in the invaginated basolateral membrane along straight column-like structures where it colocalized with NKA and barttin (Figure 2A). Whereas claudin-10b and barttin seemed to be equally distributed along the infolded membranes, NKA, although present along the entire basolateral membrane, was predominant in the outer rim, comprising about 30% of the cell height. Barttin as well as NKA staining almost reached the luminal cell membrane. Only claudin-10b itself was expressed in the TJs (Figure 2B). As cTAL cells show a mosaic pattern of claudin-10b,<sup>15</sup> some cells (Figure 2C, \*) did not express claudin-10b (Figure S2B). The absence of claudin-10b in these cells did not lead to obvious differences in NKA and barttin localization. For NKA, we analyzed this in more detail. Comparing NKA staining intensity between claudin-10b-positive and claudin-10b-negative regions within the same stained tubule, there was no difference found. cKO cTAL showed a mirror image of the claudin-10b-negative mosaic cell since in stretches of cells (approx. 15–20%) Ksp-Cre failed to excise claudin-10b (Figure 2D, #; Figure S2B). Claudin-10b presence or absence again did not change the NKA staining pattern or immunofluorescence intensity (Figure 2C–E). Western blot analysis for NKA protein showed no differences in protein expression levels between WT and cKO (Figure 2F). Western blot analysis of ion transport proteins along the nephron revealed particularly high expression of NKA and claudin-10 in TAL in comparison to PT (Figure S1, for NKA in accordance to Katz et al.<sup>33</sup>). Data on claudin-10 and barttin expression in WT compared to cKO are shown in Figure S2. Also, barttin expression did not depend on the presence of claudin-10. In cKO, claudin-16 (only expressed in TJs) and claudin-19 (also some extra-junctional expression) occupy TJs of claudin-10b-negative cells.<sup>11</sup> Hence, we checked for claudin-19 expression in WT and cKO (Figure S3). Claudin-19 immunofluorescence in infoldings was weak or even absent. Nevertheless, in WT and cKO tubules, infoldings were visible in their basolateral column-like appearance, indicating that claudin-19 might be involved but was not excluded by claudin-10b. Western blot analysis showed no difference in protein abundance, excluding a quantitative replacement of claudin-10b by claudin-19 (Figure S3E).

### Morphology of infoldings

Transmission electron microscopy was performed on ultra-thin sections of WT and cKO kidneys. Images of the inner stripe of outer medulla (ISOM) TALs were taken due to the absence of the claudin-

16/-10 mosaic.<sup>15</sup> In WT, we observed several extensive infoldings (Figure 3A, arrow) of the basolateral plasma membrane along with mitochondria. In cKO mice, the infoldings looked less structured, with wider extracellular space between them (Figure 3B, arrow; Figure S6).

### Ouabain inhibition of NKA

As an absence of claudin-10b did not alter the expression pattern of the other basolateral proteins, and since electron microscopy (EM) indicated a difference in the morphology of the infoldings, we hypothesized, that claudin-10b may have a role in the accessibility of the infoldings. We adapted technique<sup>34</sup> which is used for the opening of TJs and other protein interaction-dependent cell adhesion complexes by depleting extracellular Ca<sup>2+</sup> with EGTA. To this end, we perfused manually isolated cTALs of C57BL/6 mice and measured the transepithelial membrane voltage under control and basolateral Ca<sup>2+</sup>-free solution. The luminal solution still contained Ca<sup>2+</sup> ions to protect the TJ itself, which was not the target of this treatment. Basolateral adhesion complexes directly beneath the TJs might, therefore, have not been targeted. The Ca<sup>2+</sup>-free solution showed no significant impact on the transepithelial voltage ( $V_{te}$ ), resistance ( $R_{te}$ ), or the equivalent short-circuit current ( $I'_{sc}$ ) when compared to a control group (Figure 4A) and only a minor short-term effect on  $V_{te}$  directly after application (Figure S4). To further investigate the accessibility of the infoldings, we used the drug ouabain which has to enter the infoldings for effective inhibition of NKA. Initially, we determined the half maximal inhibitory concentration of ouabain in cTALs ( $IC_{50}$ ; original traces in Figure 4B,C), again with no differences between control and Ca<sup>2+</sup>-free solution. Consequently, the working concentration chosen was 100  $\mu$ M. To test the accessibility to NKA, we evaluated the initial speed at which the NKA inhibition took place (change of  $V_{te}$  per time, Figure 4D). Under control conditions, cTALs of BL/6 mice displayed a  $V_{te}$  change of about  $-9$  mV/min, summarized as relative inhibition speed normalized by the inhibited proportion of  $V_{te}$  ( $0.82 \pm 0.05$  1/min; Figure 4E); chelating the Ca<sup>2+</sup> increased the speed of inhibition to approx.  $-13$  mV/min and a relative inhibition speed of  $1.02 \pm 0.06$  1/min (Figure 4E). Interestingly, relative inhibition speed at wash-out was independent of basolateral Ca<sup>2+</sup> and slower, indicating a dependence on drug dilution and dissociation from the NKA instead of accessibility (Figure 4E).

As already described,<sup>11</sup> cTALs of cKO mice showed an increased  $V_{te}$  under control conditions when compared to WT (Figure 5A). As cKO also exhibited higher  $R_{te}$  values,  $I'_{sc}$  remained unaltered, that is, transcellular transport was the same but TJ properties were altered by cKO (Figure S5). For both WT and cKO, Ca<sup>2+</sup>-free conditions or time control did not lead to a change in  $V_{te}$  (Figure 5B). For ouabain inhibition, the same pattern was observed for both, WT and cKO, with varying inhibition for single individual tubules, resulting in a mean inhibition of  $\sim 50\%$  (Figure 4C). The speed of inhibition in claudin-10 cKO cTALs was strikingly higher than in WT cTAL, especially before normalization to the inhibited voltage (original traces in Figure 5D,E), but still visible after normalization (Figure 5F). The speed of ouabain wash-out was

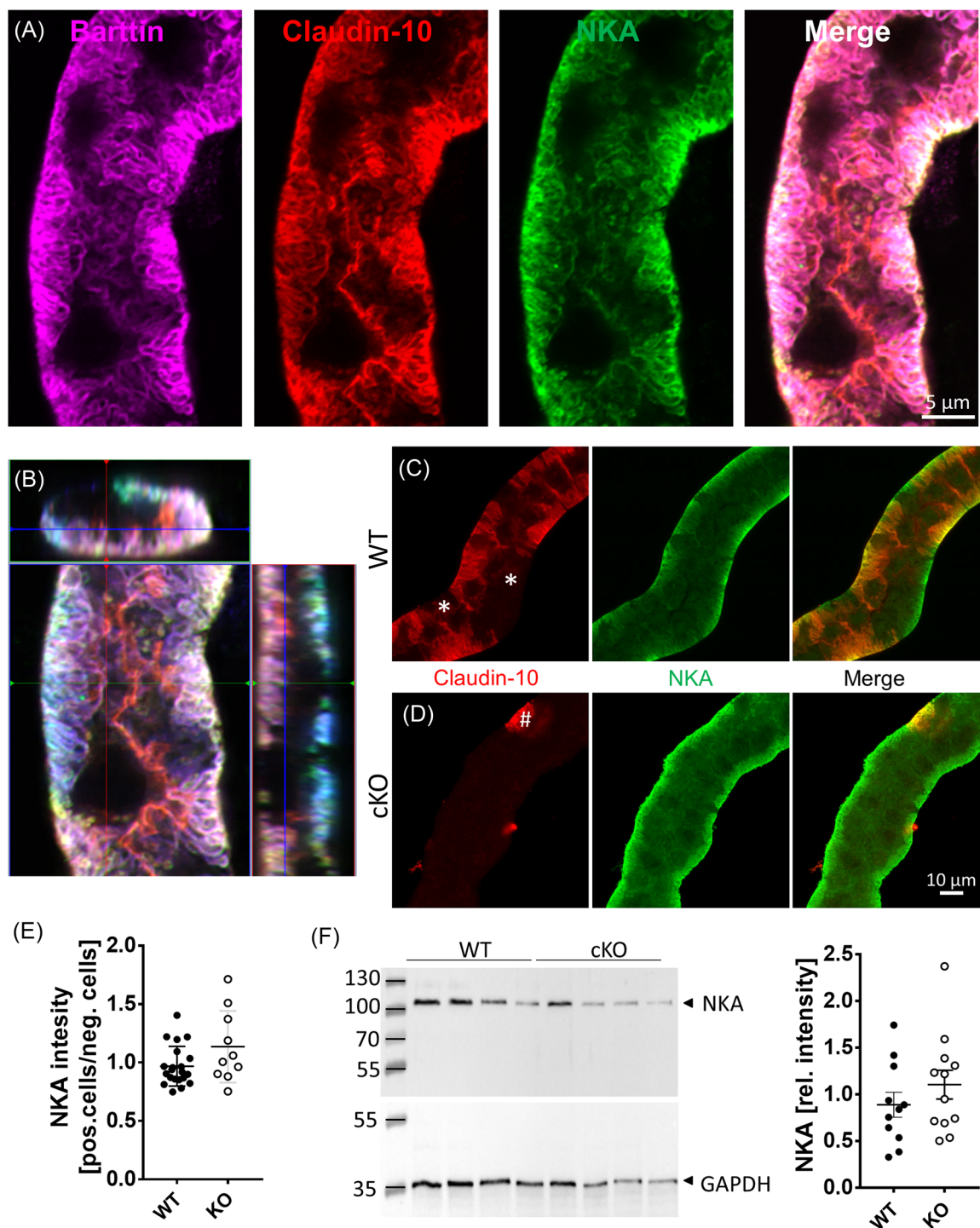


**FIGURE 2** Localization and expression of Na<sup>+</sup>-K<sup>+</sup> ATPase (NKA) in isolated mouse cTAL tubules. (A) Airyscan colocalization pattern of barttin (magenta), claudin-10 (red), and NKA (green) in the infoldings of the TAL. (B) 3D reconstruction of a collapsed triple-stained cTAL: barttin (blue) and NKA were observed deep into the infoldings, almost up to the TJs. (C,D) Immunofluorescence of claudin-10 and NKA in the cTAL of WT (C) and cKO (D) mice. In WT, some cells did not express claudin-10 (indicated by \*). In cKO, claudin-10 staining was rarely detected (indicated by #; due to failure of Ksp-Cre). In both cases, the pattern and intensity of NKA staining did not change. (E) NKA intensity given by the ratio between positive/negative claudin-10 cells in WT and cKO mice was equal. cTALs = 21 and 10 of 7 and 8 mice, respectively. (F) Quantification of NKA protein expression in cTAL samples of *n* = 11 WT and 12 cKO mice; normalization to GAPDH expression did not show any difference.

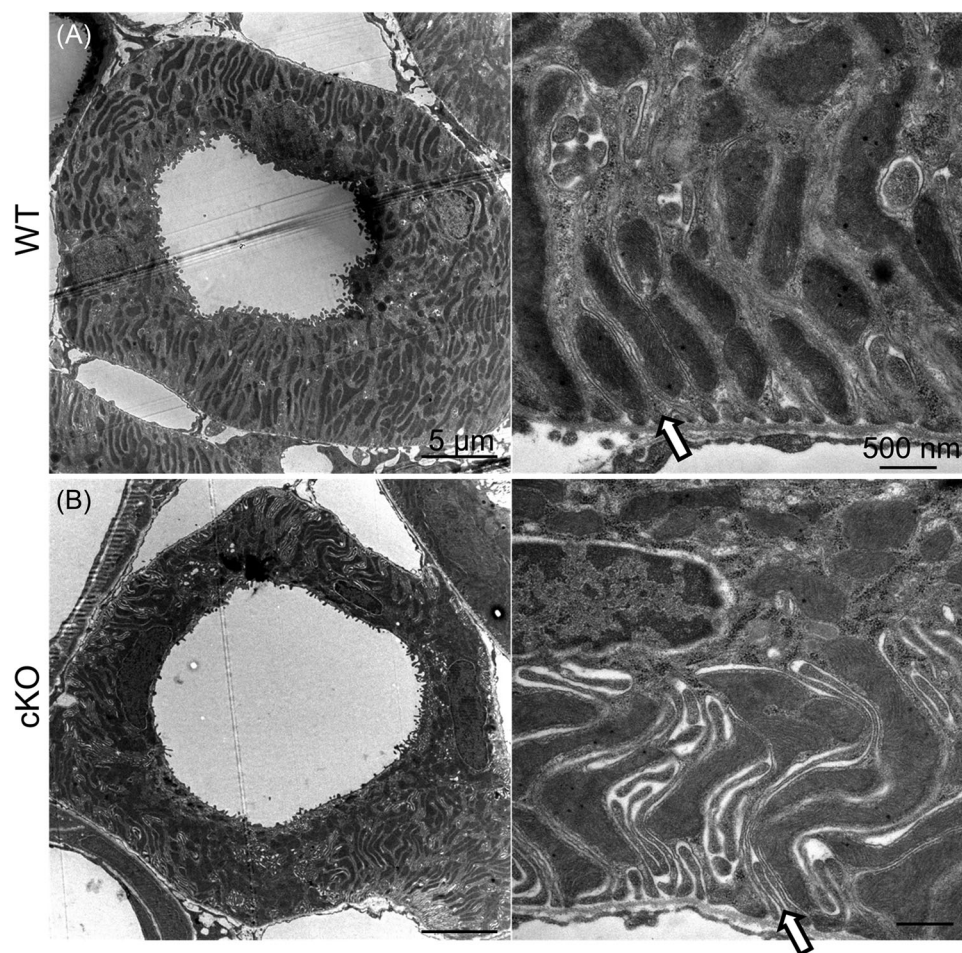


**FIGURE 3** Electron micrograph of ISOM TAL from ultra-thin kidney sections. Lower magnification (left) and a detailed picture (right). The ultrastructure of the ISOM TAL epithelia is characterized by extensive basolateral infoldings and the presence of numerous elongated mitochondria. (A) WT with deep, tightly packed basolateral infoldings parallel to the mitochondria that extend almost to the luminal membrane ( $n = 3$ ). (B) Claudin-10 cKO revealed deep infoldings; however, the structures did not present the same density pattern as for the WT and displayed a wider space between infolding structures ( $n = 3$ ). Scale bar left: 5  $\mu\text{m}$ ; right: 500 nm.

again not different between the genotype or under  $\text{Ca}^{2+}$ -free solution (Figure 5F, right).

### Fluorescein diffusion into the cTAL infoldings

Considering that claudin-10b might have an influence on the width of the infoldings and that ouabain accessibility was different in WT and cKO, we tested the free diffusion of fluorescein into the infolding space. MitoTracker dye was used to stain mitochondria and it did not colocalize with fluorescein (Figure 6A). In order to open the infoldings, we used again an extracellular  $\text{Ca}^{2+}$ -free solution. We hypothesized that if claudin-10b bridges the infoldings for stabilization, this bridging should be opened by chelation of  $\text{Ca}^{2+}$ . The kinetics of the in- and outflow of the fluorescein was too fast for the measuring approach. So, we measured remaining fluorescein after wash-out (fluorescein trapping) in the presence or absence of  $\text{Ca}^{2+}$  in a paired experimental approach, as shown in Figure 6B (Protocol 1). In both WT and cKO, residual fluorescein at 2 min after wash-out was low and independent of baso-

lateral removal of  $\text{Ca}^{2+}$  (Figure 6C). As Protocol 1 did not distinguish between high and low diffusion rates for loading and wash-out, we applied Protocol 2. We observed that the readdition of  $\text{Ca}^{2+}$ , that is, closing the infoldings before wash-out (Figure 6B, Protocol 2), led to substantial trapping of fluorescein in WT (Figure 6D), significantly increasing the fluorescein values measured 2 min after wash-out. This observation was dependent on claudin-10b since  $\text{Ca}^{2+}$ -dependent fluorescein trapping was attenuated in claudin-10 cKO mice (Figure 6D).

### DISCUSSION

We show that claudin-10b is expressed in the infoldings of the cTAL along with other important and abundant transport proteins. The absence of claudin-10b did not alter the expression level and overall distribution of these proteins, neither in claudin-10b negative cells in WT, nor after Ksp-Cre-driven deletion of claudin-10b. In functional studies, we tried to separate claudin-10b TJ function<sup>11,12,15</sup> from its putative function in the basolateral membrane.  $\text{Ca}^{2+}$  chelation,



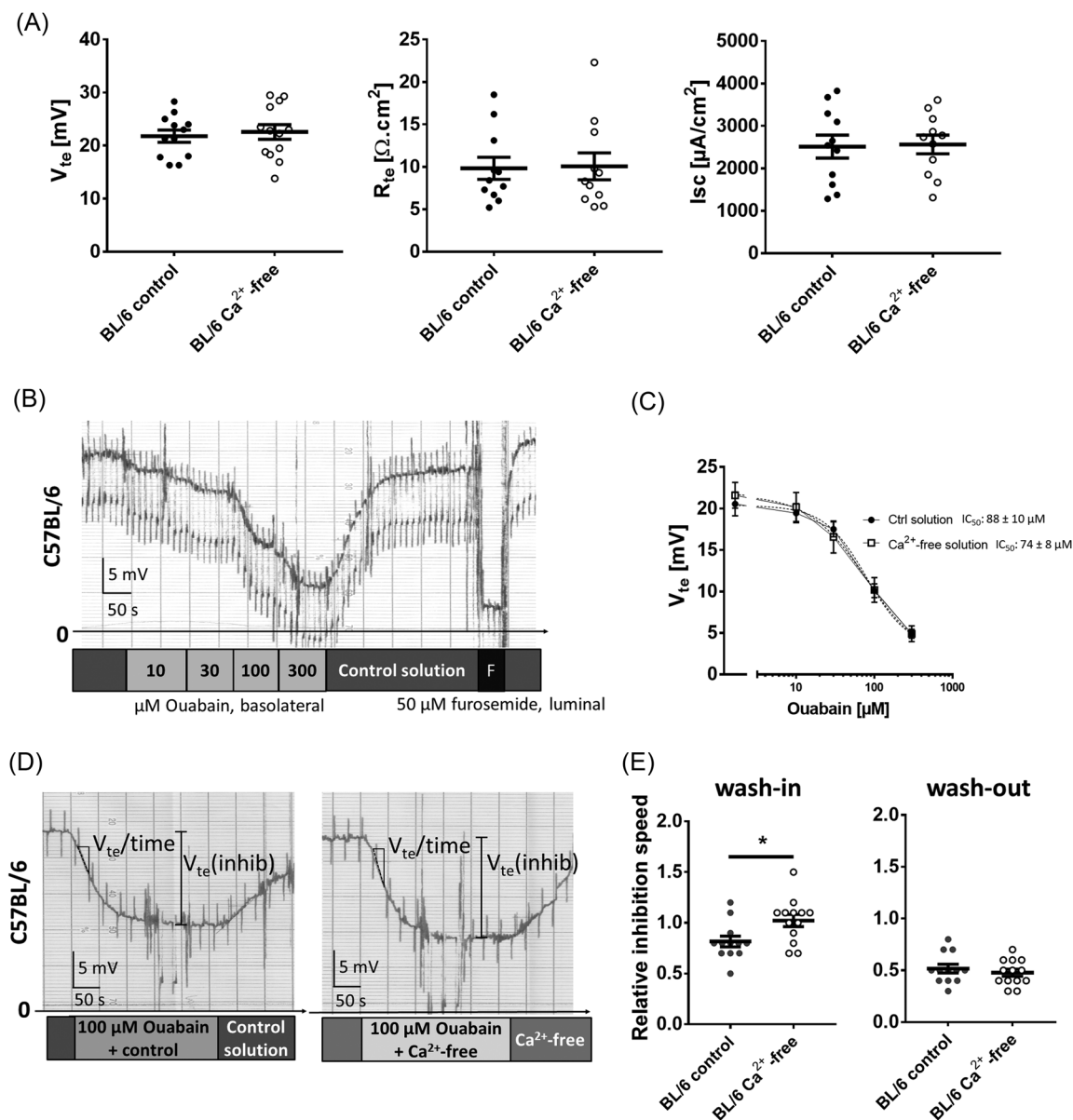


**FIGURE 4** Effect of basolateral  $\text{Ca}^{2+}$  depletion on cTAL ion transport and effect of ouabain in BL/6 mice. (A) Transepithelial transport parameters were not compromised by  $\text{Ca}^{2+}$ -free solution,  $n = 12$  and  $13$ . (B) The original recording of ouabain inhibition and luminal furosemide (F) application (voltage deflections are caused by current injection to measure  $R_{te}$ ). (C) Concentration-response curve.  $\text{IC}_{50}$  on  $V_{te}$  under control and  $\text{Ca}^{2+}$ -free solution, cTAL = 5 and 7 of  $n = 3$  and 5 mice, respectively. (D) The original recording of inhibition kinetics (injection currents partially reduced). The slope of the onset of inhibition was accelerated at low basolateral  $\text{Ca}^{2+}$ . Slope triangle ( $V_{te}/\text{time}$ ) and maximal voltage change ( $V_{te}(\text{inhib})$ ) by  $100 \mu\text{M}$  ouabain were used for the calculation of normalized relative inhibition speed. (E) Normalized relative inhibition speed by ouabain. The wash-in phase was accelerated by  $\text{Ca}^{2+}$ -free solution, while the wash-out remained slow and unaffected, cTAL = 12 and 13 of  $n = 5$  and 6 mice;  $*p < 0.05$ .

normally used to disrupt cell-cell contacts, including TJs, was used in this case only from the basolateral side to “unbutton” cell contacts in the infoldings. This procedure increased the speed by which the NKA inhibitor ouabain was able to inhibit transcellular cTAL transport. The speed was higher in the absence of claudin-10b and not further increased by the  $\text{Ca}^{2+}$ -chelating treatment. To address this phenomenon with an alternative and independent method, we flooded the infoldings with fluorescein and were able to trap the fluorescent molecules within the infoldings when reading  $\text{Ca}^{2+}$  before the

wash-out. This trapping was largely attenuated in the absence of claudin-10b. In electron microscopy, the basolateral infoldings in cKO appeared wider and less structured when compared to WT mice. Previous studies by Zampighi and Kreman as early as 1985 showed with a more sophisticated EM approach that there are indeed bridges between infolding membranes that might correlate to the claudin-10b “buttons.”<sup>18</sup>

Claudin-10b has a prominent role in TAL paracellular function as we described in Refs. 11 and 12. Lack of claudin-10b leads to the loss of the



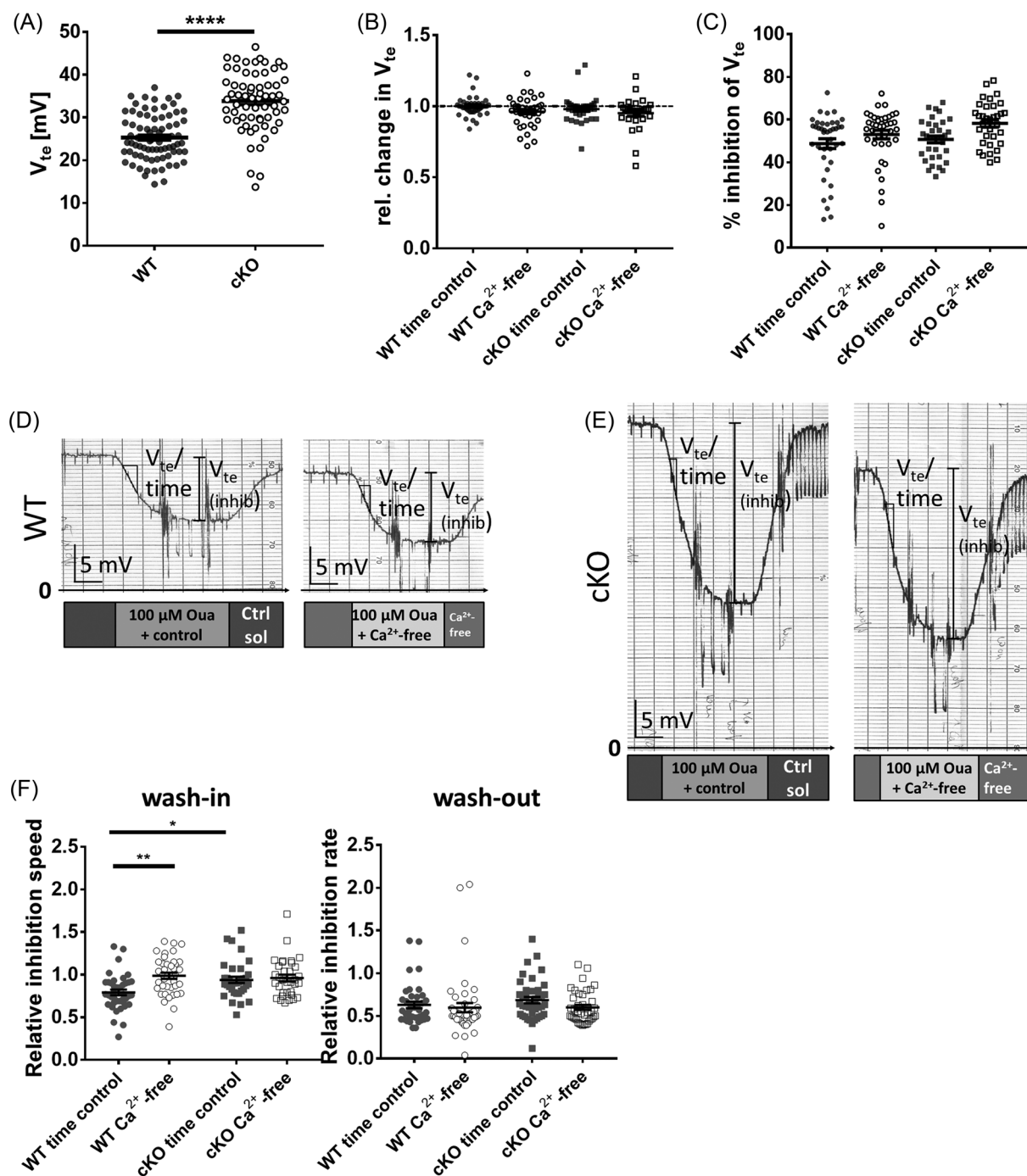


**FIGURE 5** Effect of claudin-10 cKO and basolateral  $\text{Ca}^{2+}$  depletion on cTAL ion transport and ouabain inhibition of ion transport. (A)  $V_{te}$  under control conditions was higher in cKO compared to WT; 79 WT cTALS and 64 cKO cTALS of  $n = 17$  WT and 15 cKO mice, respectively. \*\*\*\* $p < 0.0001$ . (B)  $V_{te}$  did not change with time or by basolateral  $\text{Ca}^{2+}$ -free treatment in either WT or cKO. (C) 100  $\mu\text{M}$  ouabain finally inhibited  $V_{te}$  in all groups to a similar extent. (D,E) Original chart recordings. Inhibition kinetics was accelerated in WT by  $\text{Ca}^{2+}$ -free treatment. In cKO, it was higher than in WT but independent of  $\text{Ca}^{2+}$ -free treatment. Slope triangle ( $V_{te}/\text{time}$ ) and maximal voltage change ( $V_{te}(\text{inhib})$ ) by 100  $\mu\text{M}$  ouabain) were used for the calculation of normalized relative inhibition speed. (F) Summary of the normalized relative inhibition speed. Wash-out kinetics was slower and remained unaffected by genotype or low  $\text{Ca}^{2+}$  treatment. (A,F) \* $p < 0.05$ ; \*\*\* $p < 0.001$ . (B,C,F) Data are presented as cTAL (between 29 and 40) of 15–17 mice.

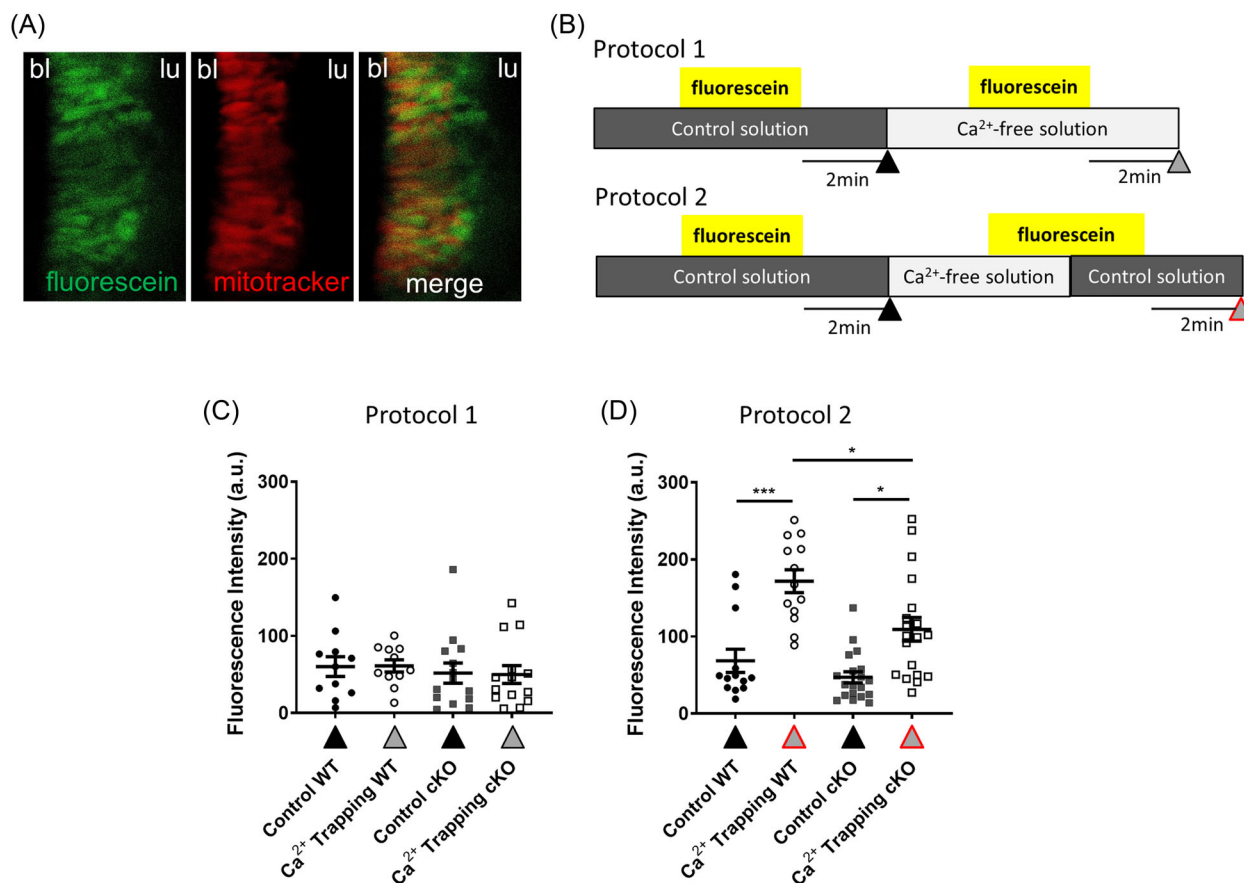


**FIGURE 6** Fluorescein trapping in the basolateral infoldings of isolated perfused cTALs. (A) Fluorescein labeling of the extracellular space formed by basolateral infoldings was separate but in close proximity to mitochondrial staining of the intracellular compartment (MitoTracker, red). (B) Experimental protocols with basolateral incubation solutions. Triangles indicate the time of fluorescein intensity measurements. (C) Fluorescein fluorescence intensity (Protocol 1) after 2 min wash-out was not influenced by Ca<sup>2+</sup>-free treatment in WT and cKO; data represent 11 and 14 cTALs of  $n = 9$  and 10 mice, respectively. (D) In Protocol 2, fluorescein was trapped in the infoldings after Ca<sup>2+</sup>-free treatment by readdition of Ca<sup>2+</sup>. The effect was larger in WT when compared to cKO; data represent 13 and 19 cTALs of  $n = 9$  WT and 10 cKO mice, respectively. \* $p < 0.05$  and \*\*\* $p < 0.001$ .

TJ mosaic, that is, the side-by-side pattern of a Na<sup>+</sup>-selective (claudin-10b) and a more divalent-selective (claudin-16, -19) TJ.<sup>15</sup> We did not measure paracellular selectivity again but could recapitulate that the NaCl transport current ( $I_{sc}$ ) was unaltered in cKO (based on the increased transepithelial resistance  $R_{te}$  by removal of a highly permeable paracellular pore and the consequently increased transepithelial voltage  $V_{te}$ ). From these electrophysiological data, we had no strong indication for a direct functional impact of basolateral claudin-10b on furosemide-inhibitable transcellular transport.

For extra-junctional claudin-19, recruitment to the TJ could be shown in collecting duct cell culture,<sup>23</sup> suggesting a role for basolateral claudin-10b also as a TJ reserve. However, we previously investigated the effect of antidiuretic hormone (ADH) on ISOM TAL and could find increased claudin-10b function in the TJ but no shift in claudin-10b localization or reduction in basolateral staining.<sup>35</sup> We, therefore, conclude that claudin-10b in the infoldings does not serve as a protein pool for the TJs but fulfills an independent task.

Claudin-10 is a tetraspanin in its molecular design (four trans-membrane regions, two extracellular loops, the ability to interact

in *cis*, ability to bind bridging or cytoskeletal proteins).<sup>36,37</sup> Therefore, another hypothesis was that claudin-10 could be involved in the recruitment and positioning of membrane transport platforms similar to the so-called tetraspanin web.<sup>36,37</sup> NKA has been described to be organized and regulated in lipid rafts;<sup>38</sup> however, we did not see a change in localization and protein amount in the absence of claudin-10.

We further hypothesized that, instead of *cis* interaction as in tetraspanin webs, claudin-10b might interact between infolded membranes in the *trans* position to stabilize the width of the invaginated extracellular space. To separate TJ and infolding function, we adapted the Ca<sup>2+</sup> switch approach, which is rather unspecific in combination with the available cKO mouse model. Ouabain concentration response was comparable to that indicated in the literature for mouse kidney,<sup>39</sup> and IC<sub>50</sub> was unaltered between genotypes and also not affected by basolateral Ca<sup>2+</sup> removal. Differences in speed of inhibition indicated better accessibility of the pump proteins under Ca<sup>2+</sup>-free conditions and in the absence of claudin-10b. Interestingly, the wash-out of the inhibitor from the restricted spaces was not affected. We speculate that the kinetics of wash-out is dominated by the time constants of

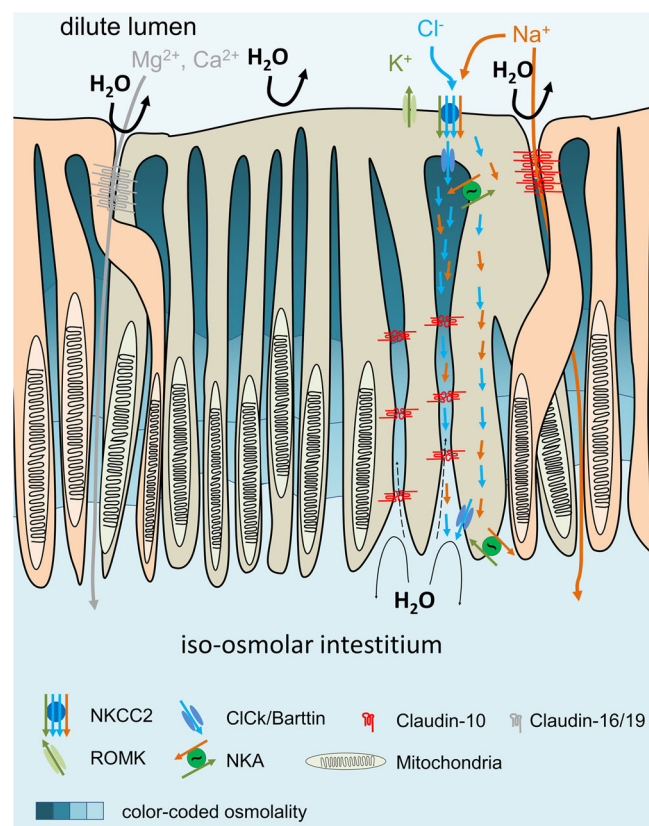


**FIGURE 7** Schema of three adjacent cTAL cells with TJs and extensive infoldings of the basolateral membrane. All cells express claudin-16/19, and the two cells on the right express claudin-10. Hence, the TJ on the left prefers divalent cations, while the TJ on the right is formed by claudin-10 and prefers  $\text{Na}^+$ . The central claudin-10-positive cell shows claudin-10 in *trans* interaction between the infolded membranes. These membranes are equipped with NKA, the chloride channel, and barttin.  $\text{Na}^+$  and  $\text{Cl}^-$  enter the cell via  $\text{Na}^+ - 2\text{Cl}^- - \text{K}^+$  cotransporter under  $\text{K}^+$  recycling. Both, the luminal membrane and the tight junctions, are watertight. Therefore, the luminal fluid is dilute, while the fluid in deeply invaginated infoldings or lateral spaces becomes hyperosmotic by continuous  $\text{NaCl}$  transport (osmolality indicated by color saturation). The basolateral interstitium is isotonic (renal cortex). We hypothesize that claudin-10 stabilizes the infoldings, hindering basolateral water influx.

receptor dissociation and dilution. Due to this observation, we further studied the ability of the infoldings to allow fluorescein diffusion inside this narrow space. The presence of claudin-10b in the infolding membrane acted as a diffusion hindrance to fluorescein, with a higher fluorescence intensity under the trapping protocol (depletion and readdition of  $\text{Ca}^{2+}$ ) in the WT.

Why would the TAL need a basolateral membrane-infolding stabilizing system? One explanation could be its apical water tightness.<sup>1</sup> In the PT, salt and water are transported almost iso-osmotically,<sup>40</sup> whereas in the TAL, luminal water does not follow the solutes.<sup>41</sup> Ions must pass transcellularly with basal outflow. Or, as the infoldings almost reach the luminal membrane, they allow a short-cut of ions from the NKCC2 import directly to the basolateral extracellular space (via  $\text{Cl}^-$  channel and pump), facilitating the continuous outflow of ions through the

entire basolateral membrane.<sup>42,43</sup> However, this should be accompanied by increasing osmotic pressure in this extracellular subdomain. As a direct effect, this osmotic pressure would drive water from the basolateral side into this narrow space and potentially disturb continuous ion flux and basolateral architecture. A claudin-10b-based stabilizing system would help keep the infoldings architecture and facilitate a high flux of the reabsorbed salt directed to the basal interstitium. This hypothesis is summarized in Figure 7.

At this stage, we cannot answer the question of whether other claudins partially substitute for the function of claudin-10 in the cKO and in claudin-10-negative mosaic TAL cells. Yet, there was no substantial take-over of the infoldings by claudin-19 although claudin-16, -19, and -3 occupied the TJs in the claudin-10 cKO. Claudin-3 or claudin-19 immunofluorescence showed extra-junctional staining of both claudins but without the distinct column-like infolding pattern.<sup>15,44</sup> Others found claudin-19 exclusively in TJs.<sup>45</sup> In isolated cTALs, we showed some claudin-10b-negative cells with claudin-19 in the infolding membrane, but not in an amount visible in overall protein expression. Our investigation of claudin-10b in the infoldings required a modified treatment of samples for immunofluorescence by slow cooking. This might have compromised the extra-junctional quantification of other claudins but allowed the staining of the infoldings in striking loops. EM fixation processes, on the other hand, might have facilitated the discovery of the widening of the infoldings (our findings) but also hindered the already described intercellular bridges.<sup>18,46</sup>

We propose a new function of claudin-10b in the basolateral infoldings of the water-tight TAL epithelium. Claudin-10b *trans* interaction between membrane invaginations of the same cell serves as a stabilizing system for the intense transcellular osmotic pressure generated by high electrolyte flow. Future investigations may reveal if the observed urine concentration defect in cKO<sup>11</sup> is partially due to the loss of this function; and will also show how this new claudin-10b function can be integrated into the growing data about TAL cell heterogeneity.<sup>15,46,47</sup>

## ACKNOWLEDGMENTS

We thank T. Stegman, R. Lingg, and the team of the animal facility of the CAU for their technical support. We thank Thomas J. Jentsch for the barttin and Jianghui Hou for the claudin-19 antibodies. We thank the members of Abberior Instruments, Janina Hanne and Jan-Gero Schloetel, for the STED image (Figure 1D) taken in Göttingen.

Open access funding enabled and organized by Projekt DEAL.

## AUTHOR CONTRIBUTIONS

C.Q. and N.H. contributed equally and performed and analyzed experiments, and contributed to the manuscript and figure preparation. S.L.S., O.V.S., L.P., and K.M. performed experiments. D.M. generated the kidney-specific (Ksp-Cre) C57BL/6 claudin-10<sup>-/-</sup> mice. T.B. contributed to the conception and manuscript preparation. D.G. and M.B. contributed to the overall design of the study and writing of the manuscript. All authors approved the final version of the manuscript.

## COMPETING INTERESTS

The authors declare no competing interests.



## ORCID

Catarina Quintanova  <https://orcid.org/0000-0001-6617-2006>

Dorothee Günzel  <https://orcid.org/0000-0002-7998-7164>

Markus Bleich  <https://orcid.org/0000-0002-1745-2295>

## REFERENCES

- Zacchia, M., Capolongo, G., Rinaldi, L., & Capasso, G. (2018). The importance of the thick ascending limb of Henle's loop in renal physiology and pathophysiology. *International Journal of Nephrology and Renovascular Disease*, 11, 81–92.
- Mount, D. B. (2014). Thick ascending limb of the loop of Henle. *Clinical Journal of the American Society of Nephrology*, 9, 1974–1986.
- Bleich, M., Schlatter, E., & Greger, R. (1990). The luminal  $K^+$  channel of the thick ascending limb of Henle's loop. *Pflügers Archiv: European Journal of Physiology*, 415, 449–460.
- Teranishi, K., & Kaneko, T. (2010). Spatial, cellular, and intracellular localization of  $Na^+/K^+$ -ATPase in the sterically disposed renal tubules of Japanese eel. *Journal of Histochemistry and Cytochemistry*, 58, 707–719.
- Ura, K., Soyano, K., Omoto, N., Adachi, S., & Yamauchi, K. (1996). Localization of  $Na^+$ ,  $K^+$ -ATPase in tissues of rabbit and teleosts using an antiserum directed against a partial sequence of the alpha-subunit. *Zoological Science*, 13, 219–227.
- Estévez, R., Boettger, T., Stein, V., Birkenhäger, R., Otto, E., Hildebrandt, F., & Jentsch, T. J. (2001). Barttin is a  $Cl^-$  channel  $\beta$ -subunit crucial for renal  $Cl^-$  reabsorption and inner ear  $K^+$  secretion. *Nature*, 414, 558–561.
- Krause, G., Winkler, L., Mueller, S. L., Haseloff, R. F., Piontek, J., & Blasig, I. E. (2008). Structure and function of claudins. *Biochimica et Biophysica Acta*, 1778, 631–645.
- Günzel, D., & Yu, A. S. L. (2009). Function and regulation of claudins in the thick ascending limb of Henle. *Pflügers Archiv: European Journal of Physiology*, 458, 77–88.
- Bleich, M., Wulfmeyer, V. C., Himmerkus, N., & Milatz, S. (2017). Heterogeneity of tight junctions in the thick ascending limb. *Annals of the New York Academy of Sciences*, 1405, 5–15.
- Milatz, S., & Breiderhoff, T. (2017). One gene, two paracellular ion channels—Claudin-10 in the kidney. *Pflügers Archiv: European Journal of Physiology*, 469, 115–121.
- Breiderhoff, T., Himmerkus, N., Stuver, M., Mutig, K., Will, C., Meij, I. C., Bachmann, S., Bleich, M., Willnow, T. E., & Müller, D. (2012). Deletion of claudin-10 (Cldn10) in the thick ascending limb impairs paracellular sodium permeability and leads to hypermagnesemia and nephrocalcinosis. *Proceedings of the National Academy of Sciences of the United States of America*, 109, 14241–14246.
- Breiderhoff, T., Himmerkus, N., Drewell, H., Plain, A., Günzel, D., Mutig, K., Willnow, T. E., Müller, D., & Bleich, M. (2018). Deletion of claudin-10 rescues claudin-16-deficient mice from hypomagnesemia and hypercalciuria. *Kidney International*, 93, 580–588.
- Milatz, S. (2019). A novel claudinopathy based on claudin-10 mutations. *International Journal of Molecular Sciences*, 20, 1–15.
- Klar, J., Piontek, J., Milatz, S., Tariq, M., Jameel, M., Breiderhoff, T., Schuster, J., Fatima, A., Asif, M., Sher, M., Mäbert, K., Fromm, A., Baig, S. M., Günzel, D., & Dahl, N. (2017). Altered paracellular cation permeability due to a rare CLDN10B variant causes anhidrosis and kidney damage. *PLoS Genetics*, 13, e1006897.
- Milatz, S., Himmerkus, N., Wulfmeyer, V. C., Drewell, H., Mutig, K., Hou, J., Breiderhoff, T., Müller, D., Fromm, M., Bleich, M., & Günzel, D. (2017). Mosaic expression of claudins in thick ascending limbs of Henle results in spatial separation of paracellular  $Na^+$  and  $Mg^{2+}$  transport. *Proceedings of the National Academy of Sciences of the United States of America*, 114, E219–E227.
- Bongers, E. M. H. F., Shelton, L. M., Milatz, S., Verkaar, S., Bech, A. P., Schoots, J., Cornelissen, E. A. M., Bleich, M., Hoenderop, J. G. J., Wetzels, J. F. M., Lugtenberg, D., & Nijenhuis, T. (2017). A novel hypokalemic-alkalotic salt-losing tubulopathy in patients with CLDN10 mutations. *Journal of the American Society of Nephrology*, 28, 3118–3128.
- Imai, M., Tsuruoka, S., Yoshitomi, K., Taniguchi, J., Suzuki, M., & Muto, S. (1999). Morphological and functional heterogeneity of the thick ascending limb of Henle's loop. *Clinical and Experimental Nephrology*, 3, 9–17.
- Zampighi, G., & Kreman, M. (1985). Intercellular fibrillar skeleton in the basal interdigitations of kidney tubular cells. *Journal of Membrane Biology*, 88, 33–43.
- Kriz, W., Kaissling, B., Schiller, A., & Taugner, R. (1979). Morphologische Merkmale transportierender Epithelien. *Klinische Wochenschrift*, 57, 967–975.
- Allen, F., & Tisher, C. C. (1976). Morphology of the ascending thick limb of Henle. *Kidney International*, 9, 8–22.
- Stoessel, A., Himmerkus, N., Bleich, M., Bachmann, S., & Theilig, F. (2010). Connexin 37 is localized in renal epithelia and responds to changes in dietary salt intake. *American Journal of Physiology*, 298, F216–F223.
- Hagen, S. J. (2017). Non-canonical functions of claudin proteins: Beyond the regulation of cell–cell adhesions. *Tissue Barriers*, 5, 1–14.
- Ziemens, A., Sonntag, S., Wulfmeyer, V., Edemir, B., Bleich, M., & Himmerkus, N. (2019). Claudin 19 is regulated by extracellular osmolality in rat kidney inner medullary collecting duct cells. *International Journal of Molecular Sciences*, 20, 4401.
- Tokuda, S., Miyazaki, H., Nakajima, K.-I., Yamada, T., & Marunaka, Y. (2010).  $NaCl$  flux between apical and basolateral side recruits claudin-1 to tight junction strands and regulates paracellular transport. *Biochemical and Biophysical Research Communications*, 393, 390–396.
- Van Itallie, C. M., & Anderson, J. M. (2013). Claudin interactions in and out of the tight junction. *Tissue Barriers*, 1, e25247.
- Hayashi, D., Tamura, A., Tanaka, H., Yamazaki, Y., Watanabe, S., Suzuki, K., Sentani, K., Yasui, W., Rakugi, H., Isaka, Y., & Tsukita, S. (2012). Deficiency of claudin-18 causes paracellular  $H^+$  leakage, up-regulation of interleukin-1 $\beta$ , and atrophic gastritis in mice. *Gastroenterology*, 142, 292–304.
- Schilpp, C., Lochbaum, R., Braubach, P., Jonigk, D., Frick, M., Dietl, P., & Wittekindt, O. H. (2021). TGF- $\beta$ 1 increases permeability of ciliated airway epithelia via redistribution of claudin 3 from tight junction into cell nuclei. *Pflügers Archiv: European Journal of Physiology*, 473, 287–311.
- Hou, J., Renigunta, V., Nie, M., Sunq, A., Himmerkus, N., Quintanova, C., Bleich, M., Renigunta, A., & Wolf, M. T. F. (2019). Phosphorylated claudin-16 interacts with Trpv5 and regulates transcellular calcium transport in the kidney. *Proceedings of the National Academy of Sciences of the United States of America*, 116, 19176–19186.
- Gong, Y., Renigunta, V., Himmerkus, N., Zhang, J., Renigunta, A., Bleich, M., & Hou, J. (2012). Claudin-14 regulates renal  $Ca^{++}$  transport in response to CaSR signalling via a novel microRNA pathway. *Embo Journal*, 31, 1999–2012.
- Greger, R. (1981). Cation selectivity of the isolated perfused cortical thick ascending limb of Henle's loop of rabbit kidney. *Pflügers Archiv: European Journal of Physiology*, 390, 30–37.
- Plain, A., Wulfmeyer, V. C., Milatz, S., Kietz, A., Hou, J., Bleich, M., & Himmerkus, N. (2016). Corticomedullary difference in the effects of dietary  $Ca^{2+}$  on tight junction properties in thick ascending limbs of Henle's loop. *Pflügers Archiv: European Journal of Physiology*, 468, 293–303.
- Kottra, G., & Frömter, E. (1983). Functional properties of the paracellular pathway in some leaky epithelia. *Journal of Experimental Biology*, 106, 217–229.
- Katz, A. I., Doucet, A., & Morel, F. (1979).  $Na$ - $K$ -ATPase activity along the rabbit, rat, and mouse nephron. *American Journal of Physiology-Renal Fluid Electrolyte Physiology*, 237, F114–F120.

34. Martinez-Palomo, A., Meza, I., Beaty, G., & Cereijido, M. (1980). Experimental modulation of occluding junctions in a cultured transporting epithelium. *Journal of Cell Biology*, 87, 736–745.
35. Himmerkus, N., Plain, A., Marques, R. D., Sonntag, S. R., Paliege, A., Leipziger, J., & Bleich, M. (2017). AVP dynamically increases paracellular  $\text{Na}^+$  permeability and transcellular NaCl transport in the medullary thick ascending limb of Henle's loop. *Pflügers Archiv: European Journal of Physiology*, 469, 149–158.
36. Caplan, M. J., Kamsteeg, E.-J., & Duffield, A. (2007). Tetraspan proteins: Regulators of renal structure and function. *Current Opinion in Nephrology and Hypertension*, 16, 353–358.
37. Charrin, S., Jouannet, S., Boucheix, C., & Rubinstein, E. (2014). Tetraspanins at a glance. *Journal of Cell Science*, 127, 3641–3648.
38. Welker, P., Geist, B., Frähauf, J.-H., Salanova, M., Groneberg, D. A., Krause, E., & Bachmann, S. (2007). Role of lipid rafts in membrane delivery of renal epithelial  $\text{Na}^+$ - $\text{K}^+$ -ATPase, thick ascending limb. *American Journal of Physiology-Regulatory, Integrative and Comparative Physiology*, 292, R1328–R1337.
39. Hebert, S. C., Culpepper, R. M., & Andreoli, T. E. (1981). NaCl transport in mouse medullary thick ascending limbs. I. Functional nephron heterogeneity and ADH-stimulated NaCl cotransport. *American Journal of Physiology*, 241, F412–F431.
40. Rosenthal, R., Milatz, S., Krug, S. M., Oelrich, B., Schulzke, J.-D., Amasheh, S., Günzel, D., & Fromm, M. (2010). Claudin-2, a component of the tight junction, forms a paracellular water channel. *Journal of Cell Science*, 123, 1913–1921.
41. Gong, Y., Himmerkus, N., Sunq, A., Milatz, S., Merkel, C., Bleich, M., & Hou, J. (2017). ILDR1 is important for paracellular water transport and urine concentration mechanism. *Proceedings of the National Academy of Sciences of the United States of America*, 114, 5271–5276.
42. Cabral, P. D., & Herrera, M. (2012). Membrane-associated aquaporin-1 facilitates osmotically driven water flux across the basolateral membrane of the thick ascending limb. *American Journal of Physiology - Renal Physiology*, 303, F621–F629.
43. Hebert, S. C. (1986). Hypertonic cell volume regulation in mouse thick limbs. II.  $\text{Na}^+$ - $\text{H}^+$  and  $\text{Cl}^-$ - $\text{HCO}_3^-$  exchange in basolateral membranes. *American Journal of Physiology*, 250, C920–C931.
44. Prot-Bertoye, C., & Houillier, P. (2020). Claudins in renal physiology and pathology. *Genes (Basel)*, 11(3), 290.
45. Angelow, S., El-Husseini, R., Kanzawa, S. A., & Yu, A. S. L. (2007). Renal localization and function of the tight junction protein, claudin-19. *American Journal of Physiology - Renal Physiology*, 293, F166–F177.
46. Chen, L., Chou, C.-L., & Knepper, M. A. (2021). Targeted single-cell RNA-seq identifies minority cell types of kidney distal nephron. *Journal of the American Society of Nephrology*, 32, 886–896.
47. Dimke, H., & Schnermann, J. (2018). Axial and cellular heterogeneity in electrolyte transport pathways along the thick ascending limb. *Acta Physiologica (Oxford)*, 223, e13057.

## SUPPORTING INFORMATION

Additional supporting information can be found online in the Supporting Information section at the end of this article.

**How to cite this article:** Quintanova, C., Himmerkus, N., Svendsen, S. L., von Schwerdtner, O., Merkel, C., Pinckert, L., Mutig, K., Breiderhoff, T., Müller, D., Günzel, D., & Bleich, M. (2022). Unrecognized role of claudin-10b in basolateral membrane infoldings of the thick ascending limb. *Ann NY Acad Sci.*, 1517, 266–278. <https://doi.org/10.1111/nyas.14882>